Design of a Reliable Bidirectional Solid-State Circuit Breaker for DC Microgrids

Xiaohui Xu, Jiamin Ye, Yu Wang, Xiaorui Xu, Ziwei Lai, and Xueyi Wei

***Abstract*—DC microgrids have drawn more and more attention in industrial applications. However, achieving efficient and reliable interruption of faults is still a challenging task in dc microgrids. In this article, a reliable bidirectional solid-state circuit breaker (RB-SSCB) is proposed for dc microgrid protection. The proposed RB-SSCB can break and rebreak bidirectional faults with no fault current surges to the source and load, and its breaking capability is stable and controllable. Consequently, when compared with the existing SSCBs, the RB-SSCB can provide more reliable protection for dc microgrids. Increased power efficiency, reduced costs, and simplified structure can also be obtained in the proposed topology. Based on circuit analysis and modeling, design guidelines for selecting the components in the RB-SSCB are given. Finally, a laboratory prototype has been built to verify the practical value and the feasibility of the proposed solution.**

***Index Terms*—Breaking capability, circuit design, microgrid protection, SCR, solid-state circuit breaker.**

I. Introduction

In recent years, the novel energy technology based on distributed generation technology has attracted more and more attention in a host of modern applications, such as photovoltaic systems, wind power generation technology, and so on [1], [2]. The direct current (dc) microgrid is regarded as a more effective access mode of distributed generation technology in comparison with the alternating current (ac) microgrid [3]–[5]. However, dc microgrids face a more difficult fault isolation problem than ac microgrids because their large fault current with high rising rate must be interrupted rapidly by circuit breakers (CBs) in the absence of current zero-crossing point [6].

Manuscript received May 6, 2021; revised August 12, 2021 and November 24, 2021; accepted December 24, 2021. Date of publication December 29, 2021; date of current version February 18, 2022. This work was supported in part by Young Creative Talents in Guangdong Province under Grant 2018KQNCX308 and in part by College Students' Innovation and Entrepreneurship Training Program under Grant XJ202113714072. Recommended for publication by Associate Editor M. S. ElMoursi. *(Corresponding authors: Xiaorui Xu; Xiaohui Xu.)*

Xiaohui Xu, Jiamin Ye, Ziwei Lai, and Xueyi Wei are with the Department of Electronic Information Engineering, Guangzhou College of Technology and Business, Guangzhou 510000, China (e-mail: xhxu1990@163.com; 844273809@qq.com; 415863263@qq.com; 2057559743@qq.com).

Yu Wang is with Public Courses Department, Hunan Traditional Chinese Medical College, Zhuzhou 412012, China (e-mail: wangyu1901@m.scnu.edu.cn).

Xiaorui Xu is with the School of Electronic Science and Engineering, University of Electronic Science and Technology of China, Chengdu 610054, China (e-mail: 81676902@qq.com).

Color versions of one or more figures in this article are available at https://doi.org/10.1109/TPEL.2021.3139110.

Digital Object Identifier 10.1109/TPEL.2021.3139110

At present, CBs can be mainly divided into three categories: 1) mechanical circuit breakers (MCBs); 2) hybrid circuit breakers (HCBs); 3) solid-state circuit breakers (SSCBs). MCBs have many disadvantages, such as long breaking time and arc generation, which will reduce reliability of dc microgrids [7]. HCBs are acceptable solutions, and have been applied in some high-voltage dc (HVdc) systems, such as Zhangbei 500 kV dc grid [8]. However, the mechanical ultrafast disconnectors (UFDs) adopted in HCBs need a long contacts separation time (several microseconds [9]), which slows the breaking speed and increasing the fault current that needs to be interrupted [10]. As a result, both MCBs and HCBs cannot well meet the high-speed and high-reliability requirements of modern dc microgrids. To provide fast and reliable protection, SSCBs, which are based on power semiconductor devices, are developed. SSCBs based on full-controlled devices (e.g., Si-IGBTs, SiC-JFETs, and GAN-HEMTs) are proposed to interrupt the fault current rapidly when the breaking command is received [11]–[15]. However, these SSCBs suffer from high conduction losses and manufacturing cost due to the use of expensive full-controlled devices with large conduction resistance.

Compared with full-controlled devices, SCRs show advantages in terms of smaller conduction losses, higher current-surge tolerance, and lower costs, thus being attractive in dc microgrid protection [16], [17]. However, due to the half-controlled characteristic of SCRs, SSCBs based on SCRs (SCR-SSCBs) need additional commutating circuits to create current zero-crossing point for SCRs, thus breaking fault currents. Early proposed SCR-SSCBs have disadvantages of slow reaction speed, high costs, no fault current limiting operation, complex structure, and control strategies [18], [19]. In [20]–[22], several SCR-SSCBs that have simpler structure and integrate the fault current limiting operation are proposed. However, these breakers only permit unidirectional fault breaking, which restricts the application in dc microgrids where require bidirectional power flow.

Through a creative reconfiguration of Z-source impedance network, bidirectional SCR-SSCBs are successively introduced [23]–[27]. In [23], an SCR-SSCB that allows bidirectional operations through a full-bridge rectifier is proposed, as shown in Fig. 1(a). However, this breaker can only be passively turned OFF in the condition that faults with high current rising rate occur, which means that its current breaking capability is uncontrollable. Besides, the conduction loss of this breaker is also high because current in each direction will flow through one SCR and two diodes. In [24], a bidirectional SCR-SSCB that can manually break current is proposed, as shown in Fig. 1(b).

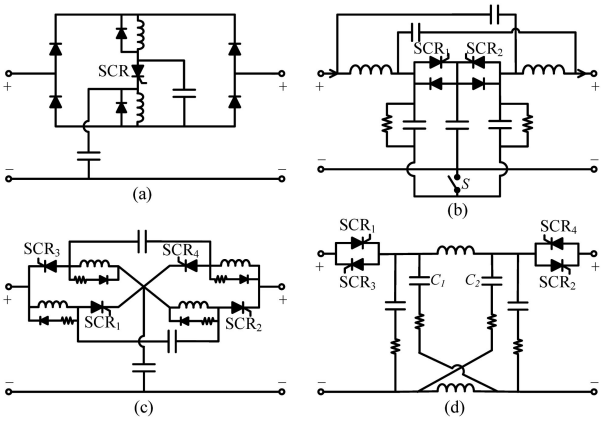

Fig. 1. Bidirectional SCR-SSCBs that use Z-source impedance networks presented in [23]–[26], respectively.

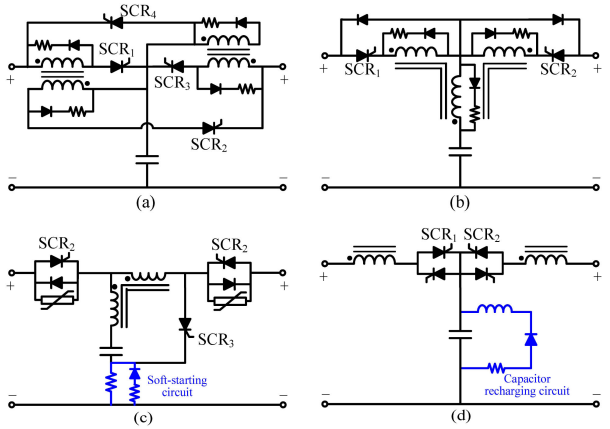

Fig. 2. Bidirectional SCR-SSCBs that use transformers proposed in [25] and [28]–[30], respectively.

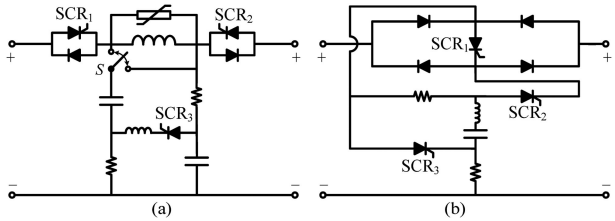

Fig. 3. Bidirectional SCR-SSCBs proposed in [33] and [34], respectively.

Moreover, its conduction loss is smaller than the former one because the system current only flow through one SCR and one diode. Nevertheless, the breaker does not provide fault rebreaking capability because its commutating capacitor (C) cannot be recharged after the breaking process. Hence, the safe restart of dc microgrids cannot be guaranteed. This shortcoming can be overcome by replacing diodes with SCRs, as shown in Fig. 1(c) and (d), which can recharge their C by triggering SCR_1 (SCR_3), and SCR_2 (SCR_4) inconsistently [25]–[27]. However, the additional SCRs will increase the breaker cost, conduction loss, and driving complexity. Besides, during current breaking process, the breakers shown in Fig. 1 will cause large current surge to the source and/or load sides (i.e., input and/or output of breaker) because their C discharges via the source and/or load sides. As the source and load usually consist of active devices, such surges may damage them.

By introducing electromagnetic effect into breaker design, bidirectional SCR-SSCBs based on transformers are proposed, which can eliminate the current surge to the source [28]–[32]. However, these breakers cannot eliminate the current surge to the load side. Moreover, for the breaker proposed in [25], two transformers are needed, which significantly increases the breaker volume, as shown in Fig. 2(a). This shortcoming can be alleviated by using a three-winding transformer, as shown in Fig. 2(b) [28]. However, this breaker does not provide low-pass filtering effect and even amplifies the input voltage at frequencies near resonance. When incorporating such SSCB into dc systems (e.g., drive systems), an additional filter will be required, thus increasing system cost and design complexity. By introducing soft-starting circuit, breaker that has low-pass filtering functionality is proposed in [29], as shown in Fig. 2(c). Besides, the use of a two-winding transformer can further reduce the breaker size. However, this breaker also does not provide rebreaker capability. In [30] and [31], another method of recharging C is proposed, which is to introduce an additional capacitor recharging circuit, as shown in Fig. 2(d). However, this breaker interrupts fault current utilizing the discharge of C, the path of which passes through the external circuit. Consequently, the current breaking capability of this breaker is unstable because it is greatly affected by the parameters of the outer circuit. If the dc system parameters or topologies are changed, this breaker may malfunction [15], [16]. Some other bidirectional SCR-SSCBs with simple structure are proposed in [33] and [34], as shown in Fig. 3(a) and (b). However, there are also some defects in these two topologies, such as causing large current surges, no rebreaking capability, and so on.

To overcome the problems existed with the existing breakers, a novel reliable bidirectional SSCB (RB-SSCB) with simple structure is proposed mainly for LVdc and MVdc microgrids. The RB-SSCB uses SCRs to enhance the power efficiency and reduce the costs of the breaker. Moreover, the RB-SSCB can interrupt current without being affected by the outer circuit parameters, and will not cause current surges to the source and load sides. Besides, the RB-SSCB also offers low-pass filtering functionality, manual breaking, and rebreaking capabilities. Consequently, compared with the previous approaches, the RB-SSCB can provide more reliable protection for dc microgrids. The operation principle and modeling of the RB-SSCB are presented in Section II, which offers the design guidelines to correctly select the circuit components of the RB-SSCB. Based on design guidelines, two design cases are carried out by simulation and laboratory experiments in Section III. Section IV gives a detailed comparison between the RB-SSCB and the existing bidirectional SSCBs. Finally, Section V concludes this article.

II. Circuit Analysis and Modeling

As can be seen in Fig. 4, the proposed RB-SSCB can be divided into three paths as follows.

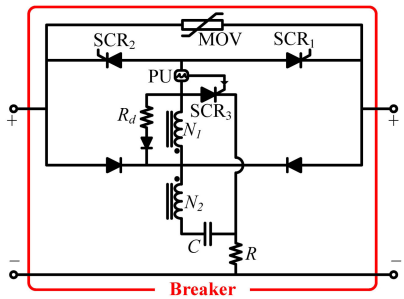

Fig. 4. Topology of the proposed RB-SSCB.

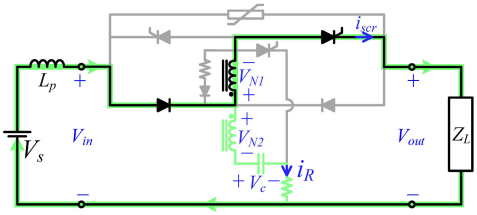

Fig. 5. Normal state of the RB-SSCB in forward power flow.

1) The main current path composed of two SCRs, two diodes, the primary winding of the transformer (N_1), and the protecting unit (PU).
2) The commutating path composed of SCR_3, the secondary winding of the transformer (N_2), a commutating capacitor (C), and charging resistance (R).
3) The snubber path composed of a Diode-R_d pair and metal oxide varistor (MOV).

Note that in addition to MOV, other snubber circuits (e.g., *RC* path) can also be used in the RB-SSCB. Because of the symmetrical structure of the RB-SSCB, the circuit analysis and modeling focus on the forward power flow, where the left port is connected to the power supply and the right port feeds the load.

A. Normal State

Fig. 5 shows the normal state of the RB-SSCB, of which the rated current ($I_{\rm rate}$) flows through the main current path to power the load. As can be seen, $I_{\rm rate}$ just flows through one SCR and diode, which can enhance power efficiency of the RB-SSCB when compared with some SSCBs where $I_{\rm rate}$ will flow through two SCRs, or one SCR and two diodes [23], [34].

In this state, voltage transfer functions are important because they can identify the filtering characteristics and stability issues of the RB-SSCB, especially when protecting active loads. With the current and voltage polarities defined in Fig. 5, one can be obtained by neglecting the ON-state resistances of the power devices

$$\begin{cases} V_{\rm in}(s) = V_{N1}(s) + V_{\rm out}(s) \\ V_{\rm in}(s) = V_{N2}(s) + \frac{i_R(s)}{sC} + Ri_R(s). \end{cases} \tag{1}$$

On the output port, Ohm's law states

$$V_{\rm out}(s) = Z_L i_{\rm scr}(s). \tag{2}$$

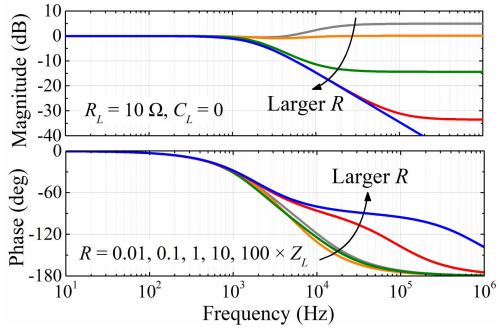

Fig. 6. Bode diagram of the $V_{\rm in}$-$V_{\rm out}$ voltage transfer functions.

where Z_L is the load impedance. Besides, the Laplace transform of the transformer terminal equations can be written as

$$\begin{bmatrix} V_{N1}(s) \\ V_{N2}(s) \end{bmatrix} = s \begin{bmatrix} L_{11} & L_{12} \\ L_{12} & L_{22} \end{bmatrix} \begin{bmatrix} i_{\rm scr}(s) \\ i_R(s) \end{bmatrix} \tag{3}$$

where L_{11} and L_{22} are the primary and secondary self-inductances, respectively, and L_{12} is the mutual inductance. By neglecting the leakage inductance of the transformer, L_{12} is

$$L_{12} = \sqrt{L_{11}L_{22}}. \tag{4}$$

Combining (1)–(4) together leads to the input–output voltage transfer function

$$\frac{V_{\rm out}(s)}{V_{\rm in}(s)} = \frac{(L_{22} - L_{12})Cs^2 + RCs + 1}{(L_{22} + RL_{11}/Z_L)Cs^2 + (RC + L_{11}/Z_L)s + 1}. \tag{5}$$

Fig. 6 shows the voltage transfer functions of the RB-SSCB. It can be seen that the RB-SSCB features unity gain at low frequencies and decaying gain at high frequencies when R is chosen larger than ten times the load resistance ($R_L = V_s/I_{\rm rate}$). This indicates that the RB-SSCB features low-pass filtering functionality, which is helpful to reduce the harmonic component, and thus protects sources and active loads.

B. Current Breaking State

When a fault occurs, the fault current will exceed preset threshold (I_T) of the PU rapidly. After that, the PU will generate a signal to trigger the SCR_3 in the commutating path, and thus, the RB-SSCB will operate in the current breaking state, as shown in Fig. 7(a). In this state, C will discharge into N_2, and thus, induce a transient voltage in N_1. This induced voltage will apply a reverse voltage stress to the SCR_1, thus forcing the device to turn OFF. As a result, the most important issue in this state is to ensure that the duration of the reverse voltage on the SCR_1 must be larger than the intrinsic recovery time of the device (t_q), thus turning OFF the SCR_1 successfully.

In this state, the R path can be seen as open circuit due to the current limitation of large R. Hence, the initial capacitor voltage maintains the source voltage (i.e., $V_{c0} = V_s$). With the current and voltage polarities defined in Fig. 7(a), one can be obtained according to KVL

$$\begin{cases} V_{\rm scr} = V_{\rm in} - V_{\rm out} - V_{N1} \\ V_c = V_{N1} - V_{N2}. \end{cases} \tag{6}$$

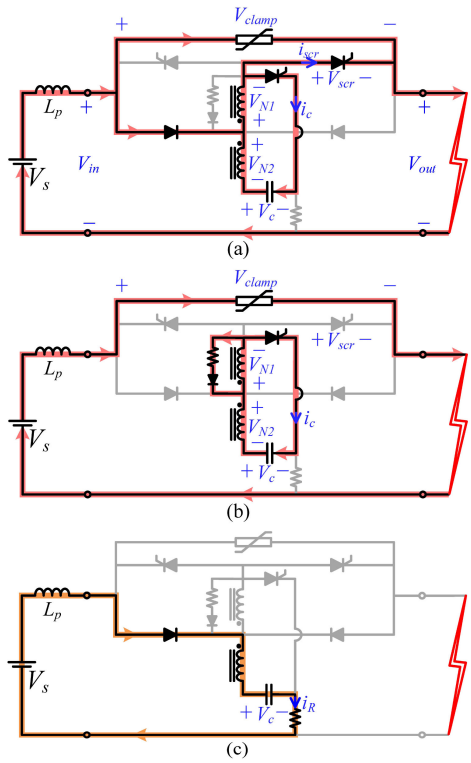

Fig. 7. Various modes of operations of the RB-SSCB in forward power flow. (a) Current breaking state. (b) Freewheeling state. (c) Recharging state.

Due to the voltage clamping function of the MOV and the electromagnetic coupling effect of the transformer, one can be expressed as

$$\begin{cases} V_s \le V_{\text{in}} - V_{\text{out}} \le V_{\text{clamp}} \\ V_{N1} = nV_{N2} \end{cases} \tag{7}$$

where V_{clamp} is the clamping voltage of the MOV and V_{clamp} is commonly 1.2–2 V_s according to the MOV characteristics [35]. n is the turns ratio of the transformer. Equations (6) and (7) indicate that larger V_{clamp} will make it more difficult for V_{scr} to drop to a negative value. Hence, the most challenging condition happens at $V_{\text{clamp}} = 2\ V_s$, which is used to derive the following equations.

By substituting (7) into (6), the initial V_{scr} at the most challenging condition can be derived as

$$V_{\text{scr0}} \le \frac{n-2}{n-1} V_s. \tag{8}$$

To turn OFF the SCR_1, V_{scr0} should be negative. Therefore, n should meet

$$1 < n < 2. \tag{9}$$

Besides, the peak transient voltages of N_1 and N_2 are

$$\begin{cases} V_{N1\_\text{peak}} = \frac{nV_s}{n-1} \\ V_{N2\_\text{peak}} = \frac{V_s}{n-1}. \end{cases} \tag{10}$$

In the meantime, i_{scr} will drop from I_T to 0 (i.e., $\triangle i_{\text{scr}} = -I_T$). Hence, the initial i_c can be derived as

$$i_{c0} = \Delta i_c = \frac{n}{n-1} I_T. \tag{11}$$

After that, i_{scr} maintains 0 and C continues to discharge in the C-N_2-N_1-SCR_3-C loop. One can be expressed by KVL

$$V_c + (n-1)^2 C L_{22} \frac{d^2 V_c}{dt^2} = 0. \tag{12}$$

Solving (12) with the initial conditions yields

$$\begin{cases} V_c = V_s \cos \beta t - \frac{nI_T}{C\beta(n-1)} \sin \beta t \\ i_c = V_s C \beta \sin \beta t + \frac{nI_T}{n-1} \cos \beta t \end{cases} \tag{13}$$

where

$$\beta = \frac{1}{(n-1)\sqrt{CL_{22}}}. \tag{14}$$

Equation (13) indicates that V_c decreases with time. Hence, the voltage rating of C should be selected equal or slightly larger than V_s. In addition, the peak value of i_c can also be calculated from (13).

Furthermore, substituting (13) into (6), and simplifying by Taylor formula obtains

$$V_{\text{scr}} = \frac{1}{n-1} \left[\frac{nV_s t^2}{2(n-1)^2 C L_{22}} + \frac{n^2 I_T t}{(n-1)C} + (n-2)V_s \right]. \tag{15}$$

For a successful turn-OFF of the SCR_1, V_{scr} should retain negative until the device finishes its reverse recovery process. Hence, a reliable turn-OFF of the SCR_1 can be guaranteed by

$$\frac{nV_s {t_q}^2}{2(n-1)^2 C L_{22}} + \frac{n^2 I_T t_q}{(n-1)C} + (n-2)V_s \le 0 \tag{16}$$

where t_q is the intrinsic recovery time of the SCR_1. Consequently, C can be determined as

$$C \ge \frac{nt_q}{(2-n)(n-1)} \left[\frac{t_q}{2(n-1)L_{22}} + \frac{nI_T}{V_s} \right]. \tag{17}$$

It can be indicated from the modeling that only V_s and the breaker parameters will affect the current breaking capability of the RB-SSCB. As a result, if the RB-SSCB is designed according to the most challenging condition (i.e., $V_{\text{clamp}} = 2\ \text{V}_s$), the breaker can provide stable current breaking capability without being affected by the parameters of the outer circuit, such as the dc system inductance and capacitance. Moreover, Fig. 8 gives the relationships among t_q and L_{22}, C, which are calculated according to (17). Since t_q of SCR that operates at tens to thousands of amperes are usually tens to hundreds of microseconds, Fig. 8 can guide the choice of C and L_{22} in practical RB-SSCB design.

C. Freewheeling State

Since C keeps discharging in the C-N_2-N_1-SCR_3-C loop located inside the breaker, no current surges will be generated to the source and load sides, which means that the source and load can be effectively protected by the breaker. As the discharging process progresses, the consumption circuit consisting

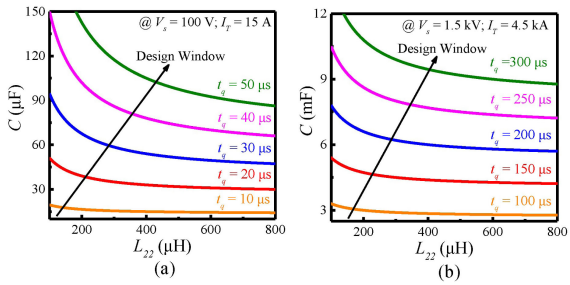

Fig. 8. Influence of t_q on the selection of C and L_{22} at (a) $V_s = 100$ V, $I_T = 15$ A; (b) $V_s = 1.5$ kV, $I_T = 4.5$ kA. In this case, n is set to 1.5, which meets (9).

of R_d and diode will turn ON once di_c/dt becomes negative. Then, the residual energy stored in L_{11} will be consumed by the consumption circuit. In the same time, the system residual energy will also be consumed through the MOV, as shown in Fig. 7(b). The consumption of the residual energy will cause a voltage overshoot in the SCR_1, which can be expressed as

$$V_{\rm scr} = V_{\rm clamp} - V_{N1} \tag{18}$$

where V_{N1} depends on the value of R_d. Typically, R_d is chosen with a resistance less than 20% of $V_s/I_{\rm rate}$, which will lead to $V_{N1} >$ -0.4 V_s [33]. Hence, for the RB-SSCB, the blocking capability ($U_{\rm DRM}$) of the SCRs should meet

$$U_{\rm DRM} \geq V_{\rm clamp} + 0.4V_s. \tag{19}$$

Finally, the discharging process of C will be completed under an underdamped condition due to the lack of resistance in this loop. This will naturally turn OFF SCR_3 at zero-crossing point of i_c. Besides, since C will also support a negative voltage at this time, nonpolarized capacitors should be used.

D. Recharging State

After the SCR_3 is naturally turned OFF, the RB-SSCB operates in the recharging state, as shown in Fig. 7(c). In this state, C will be automatically recharged to V_s through the source. After a period of system recovery (usually hundreds of milliseconds [36]), the RB-SSCB will receive the reclosing command and turn ON the SCR_1 again. If the fault still exists, the RB-SSCB will rebreak the fault. Otherwise, the RB-SSCB will work in the normal state. Because automatic reclosing and rebreaking of breakers can effectively protect microgrids under faults (especially temporary faults [37]) and guarantee the transmission efficiency of dc power, it is vital for breakers to provide rebreaking capability before reclosing [25], [30].

E. Design Guidelines

According the analysis and modeling, the design guidelines of the RB-SSCB are provided.

1) Determine the MOV and I_T of the PU considering the power rating and overload capacity of dc microgrids.
2) Select $R \geq 10\ V_s/I_{\rm rate}$ to ensure the low-pass filtering functionality of the RB-SSCB. Besides, $R_{\rm d} < 0.2\ V_s/I_{\rm rate}$ is suggested to bypass the overvoltage on the SCRs.

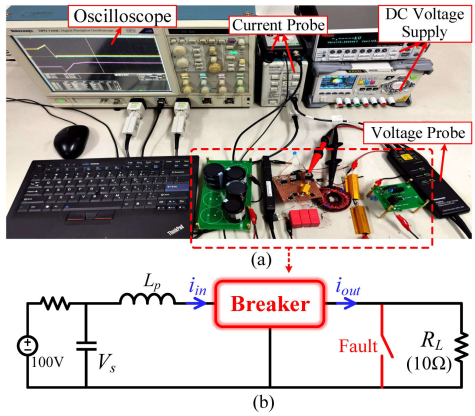

Fig. 9. (a) Laboratory prototype and (b) test circuit diagram of the RB-SSCB.

3) Choose SCRs according to (19) and $I_{\rm rate}$ of dc systems (*i.e.*, $I_{T(AV)M} \geq I_{\rm rate}$).
4) Select n according to (9). Then, C and L_{22} can be determined referring to (17). Furthermore, the transient current and voltage peaks of transformer and C can also be determined according to (10) and (13).

III. Breaker Design and Verification

Based on the design guidelines, two breaker cases are designed in this section to validate the feasibility of the RB-SSCB. The superiorities of the RB-SSCB are also evaluated by the comparison between the RB-SSCB and the previously proposed breaker (TBCB) [33].

A. Low-Voltage Design

First, a 100-V/1000-W experimental prototype has been built, as shown in Fig. 9. In this setup, a large capacitor is precharged to 100 V and used as a dc voltage source. The load resistance (R_L) is set to 10 Ω. Besides, a serious short-circuit fault can be manually induced by closing the fault switch.

According to the design guidelines, a 100 V MOV (*07D121K*) with $V_{\rm clamp}$ of 160 V is chosen and I_T is set to 15 A, i.e., 150% $I_{\rm rate}$. R of 100 Ω and R_d of 1 Ω are selected. According to (19), a 200-V/10-A SCR (*2N6402G*) with t_q of 20 μs is selected. From (9), n of 1.5 can be obtained. Then, $L_{22} = 255$ μH and $C = 45$ μF are chosen, which meets the requirement of (17). The detailed parameters are summarized in Table I.

B. Experimental Verification

The designed breaker was first tested under the dc environment that has very low system parasitic inductance (L_p), such as dc shipboard systems [38]. The experimental waveforms of the RB-SSCB are shown in Fig. 10. It can be seen in Fig. 10(a) that both the input current ($i_{\rm in}$) and the output current ($i_{\rm out}$) of the RB-SSCB rise to I_T rapidly after the fault occurs. After that, the SCR_3 is triggered. This causes C to discharge in the C-N_2-N_1-SCR_3-C loop, and thus, induces a transient voltage in N_1 through the electromagnetic coupling effect of the transformer at the same time. This induced voltage is reversely imposed on

TABLE I
DETAILED BREAKER PARAMETERS

Component	Parameter	Value
PU	I_T	15 A
MOV	V_{DC}	100 V
	V_{clamp}	160 V
	U_{DRM}	200 V
SCR	$I_{T(AV)M}$	10 A
	t_q	20 μs
Resistor	R	100 Ω
	R_d	1 Ω
Transformer	L_{11}	592 μH
	L_{12}	380 μH
	L_{22}	255 μH
Capacitor	C	45 μF

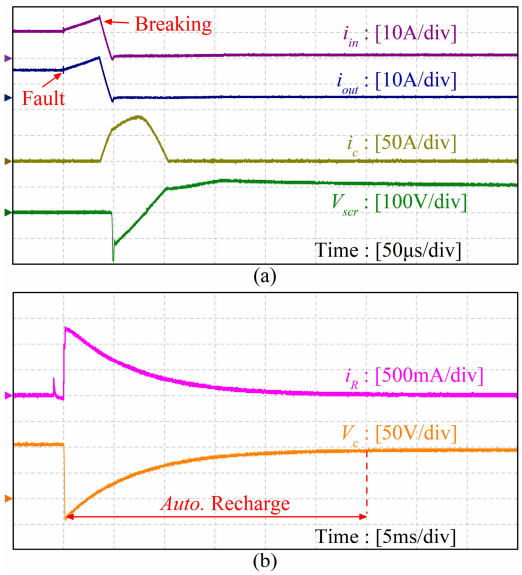

Fig. 10. Measured waveforms of (a) $i_{\rm in}$, $i_{\rm out}$, i_c, and $V_{\rm scr}$, and (b) i_R, and V_c at $L_p = 5$ μH.

the $\rm SCR_1$, making $V_{\rm scr}$ change to a negative value and the $\rm SCR_1$ turn OFF. Moreover, differing from the existing bidirectional SCR-SSCBs, Fig. 10(a) also illustrates that after the breaking process is triggered, both $i_{\rm in}$ and $i_{\rm out}$ of the RB-SSCB drop to zero quickly without any fault current surge. This means that when a proper I_T is chosen, the RB-SSCB can effectively protect dc sources and loads, especially those composed of power electronic devices. After that, the residual energy stored in the magnetic components (N_1 and L_p) is consumed, causing a ~25 V voltage overshoot in $\rm SCR_1$. Note that due to a small L_p, the MOV does not work in this case. In the meantime, as shown in Fig. 10(b), C discharges under an underdamped condition due to the absence of resistance in the C-N_2-N_1-$\rm SCR_3$-C loop, which can naturally turn OFF the $\rm SCR_3$ when completing this process. Finally, C is automatically recharged through the V_s-L_p-D_1-N_2-C-R-V_s loop, thereby offering breaking capability again.

Apart from some special dc systems with compact integration, breakers, and loads of modern dc microgrids are usually connected to sources through transmission lines, where the cable

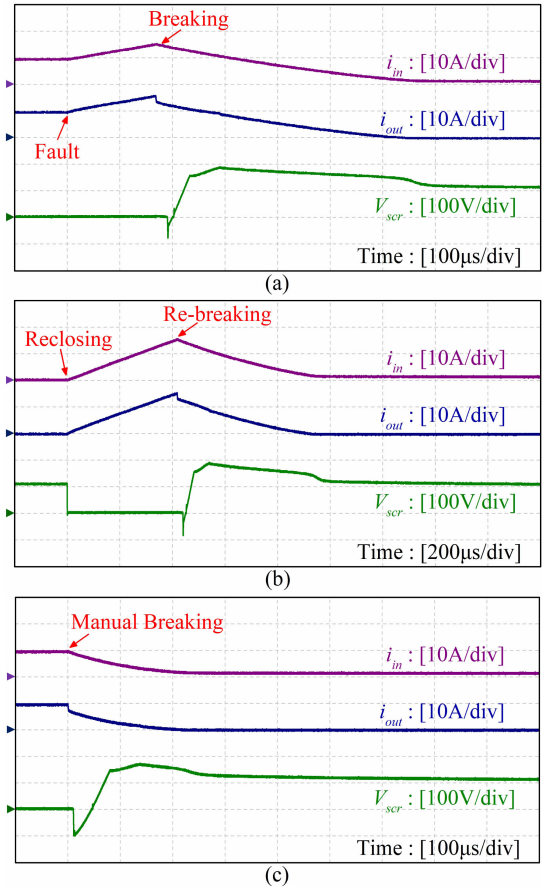

Fig. 11. Measured. (a) Fault-breaking. (b) Rebreaking. (c) Manual breaking waveforms of the RB-SSCB at $L_p = 2.2$ mH.

inductance can reach several millihenries [39]. For illustrative purpose, the RB-SSCB was further tested at $L_p = 2.2$ mH, which evaluated the stable breaking capability of the breaker. Fig. 11(a) gives the fault-breaking waveforms of the RB-SSCB. In this setup, the energy releasing of the large L_p causes the voltage clamping function of the MOV. As a result, the overshoot of $V_{\rm scr}$ exceeds 180 V, which is larger than that in Fig. 10(a). As analyzed previously, the RB-SSCB is more difficult to interrupt faults at this condition. However, since the circuit components are correctly selected according to the design guidelines, the RB-SSCB can successfully isolate the fault.

Because reclosing and rebreaking operations of the breaker can effectively reduce the adverse effect of temporary faults [25], [30], the reclosing and rebreaking operations of the RB-SSCB were tested, as shown in Fig. 11(b). In this experiment, the $\rm SCR_1$ was reclosed when the fault still existed. As a result, both $i_{\rm in}$ and $i_{\rm out}$ increase immediately once the $\rm SCR_1$ is turned ON. Since C had been automatically recharged to V_s, the RB-SSCB can successfully rebreak the fault again.

The manual breaking operation is also an important feature to the breakers in that it reflects the controllability of the breaker. As shown in Fig. 11(c), the RB-SSCB is successfully turned OFF by sending a manual breaking signal to the $\rm SCR_3$. Consequently, the RB-SSCB can be purposely switched OFF by gating the $\rm SCR_3$, then, switched ON again by gating $\rm SCR_1$.

TABLE II
PARAMETERS OF THE 1.5-KV/4.5-MW RB-SSCB AND TBCB

Component	RB-SSCB	TBCB [33]
PU	$I_T = 4.5$ kA	$I_T = 4.5$ kA
MOV	$V_{DC} = 1.5$ kV $V_{clamp} = 2.4$ kV	$V_{DC} = 1.5$ kV $V_{clamp} = 2.4$ kV
Resistor	$R = 5\ \Omega$	$R_1 = R_2 = 5\ \Omega$
Inductor	$L_{11} = 592\ \mu$H $L_{12} = 380\ \mu$H $L_{22} = 255\ \mu$H	$L_1 = 700\ \mu$H $L_2 = 50\ \mu$H
Capacitor	$C = 6.8$ mF	$C_1 = C_2 = 8$ mF

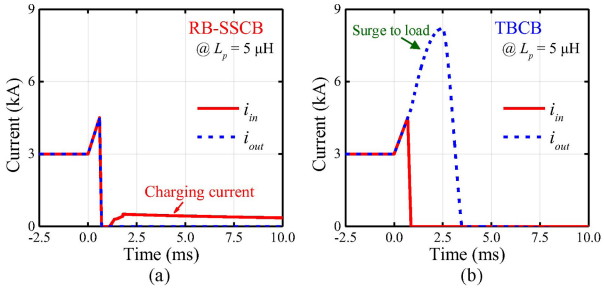

Fig. 12. Simulated breaking waveforms. (a) RB-SSCB. (b) TBCB at $L_p = 5\ \mu$H.

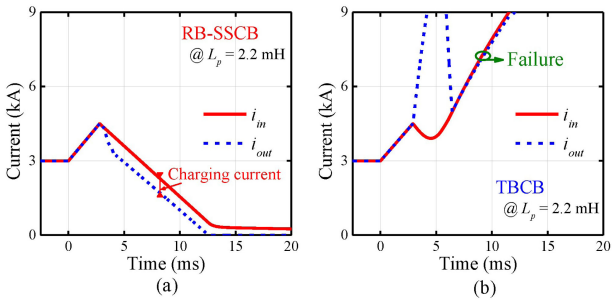

Fig. 13. Simulated breaking waveforms. (a) RB-SSCB. (b) TBCB at $L_p = 2.2$ mH.

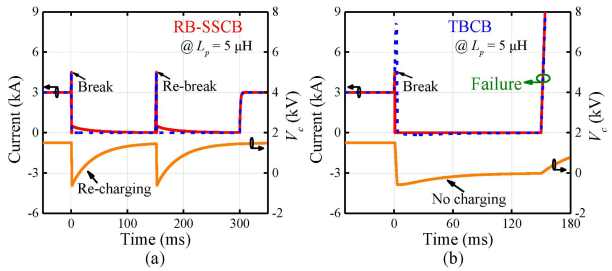

Fig. 14. Simulated breaking and rebreaking waveforms. (a) RB-SSCB. (b) TBCB at $L_p = 5\ \mu$H.

C. Medium-Voltage Design

City subway systems usually utilize dc power supplies with a voltage level of 1.5 kV, which has also been applied for photovoltaic systems and dc microgrids in Finland [40], [41]. As a result, a 1.5-kV/4.5-MW RB-SSCB was further designed and compared with the previously proposed TBCB [see Fig. 3(a)], because the TBCB can also be used in MVdc applications [33]. According to the design guidelines, two 3300-V/1800-A SCR modules (*C783CC*) with $t_q = 200\ \mu$s are used in parallel. The rest circuit components, which can be calculated following the design guidelines, are listed in Table II. Note that the parameters of the TBCB are obtained from [33]. The breakers are modeled in MATLAB/Simulink and tested under a short-circuit fault.

Fig. 12 shows the breaking waveforms of the breakers operating at $L_p = 5\ \mu$H. It can be seen that both breakers can successfully interrupt the short-circuit fault. However, a significant difference exists between the output current ($i_{\rm out}$) of the breakers. For the RB-SSCB, no fault current surge will be reflected to the load. Nevertheless, $i_{\rm out}$ of the TBCB shows large fault current surge, which may damage loads, especially those composed of power electronic converters.

The breaking waveforms of the breakers that consider the impact of large L_p are shown in Fig. 13. In this case, L_p of 2.2 mH is chosen. It can be seen that the TBCB is failed to isolate the fault under this condition, which means that its breaking capability is affected by the parameters of the outer circuit. However, the RB-SSCB can successfully interrupt the fault, which validates the reliability of the proposed solution.

Fig. 14 shows the breaking and rebreaking waveforms of the breakers operating under the temporary fault condition [37]. For an intuitive explanation, the duration of the temporary fault is set to 250 ms and the automatic reclosing time of the breakers is set to 150 ms. It can be seen that, when the fault occurs at $t = 0$ ms, both breakers can successfully interrupt the fault. After that, the RB-SSCB can automatically recharge C to provide rebreaking capability. As a result, when the RB-SSCB receives reclosing command at $t = 150$ ms, the RB-SSCB can rebreak the fault. Since the temporary fault disappears at $t = 250$ ms, the system returns to normal operation after the RB-SSCB receives the reclosing command at $t = 300$ ms. It can be concluded that the automatic reclosing and rebreaking operations of the RB-SSCB can protect microgrids from being damaged by the fault and guarantee the efficient transmission of dc power. However, the TBCB cannot charge C to provide rebreaking capability. As a result, when the TBCB receive the reclosing command at $t = 150$ ms, the breaker is failed to rebreak the fault. This is fatal because the rising fault current will damage dc microgrids rapidly.

IV. COMPARISON AND DISCUSSION

This section compares the RB-SSCB with the existing SSCBs to evaluate the superiorities of the proposed breaker.

A. Compared With SSCBs Based on SCR

Since SCR is a half-controlled device, realizing stable, and reliable current breaking capability is one of the most crucial issue for SCR-SSCB. To verify the reliability of the proposed solution, Table III compares the key features of existing SCR-SSCBs, including the topologies presented in Figs. 1–3, as well as the proposed RB-SSCB. It can be seen that the number of circuit components used in RB-SSCB is relatively small, which means that the breaker has the advantages of simple and compact

TABLE III
COMPARISON OF DIFFERENT BIDIRECTIONAL SSCBS

Category	Fig.1(a)	Fig.1(b)	Fig.1(c)	Fig.1(d)	Fig.2(a)	Fig.2(b)	Fig.2(c)	Fig.2(d)	Fig.3(a)	Fig.3(b)	**Fig.4**
Number of SCRs	1	2	4	4	4	2	3	4	3	3	**3**
Number of Diodes	6	2	4	0	4	5	3	1	2	4	**3**
Number of capacitors	2	5	3	4	1	1	1	1	2	1	**1**
Number of inductors [a]	2	2	4	2	2	1	1	1	2	1	**1**
Surge to source side [b]	$5\times I_{rate}$	$2\times I_{rate}$	$10\times I_{rate}$	Zero	Zero	Zero	Zero	Zero	Zero	$15\times I_{rate}$	**Zero**
Surge to load side [b]	$11\times I_{rate}$	$4\times I_{rate}$	$20\times I_{rate}$	$5\times I_{rate}$	$13\times I_{rate}$	$20\times I_{rate}$	$7\times I_{rate}$	$13\times I_{rate}$	$20\times I_{rate}$	$15\times I_{rate}$	**Zero**
Low-pass filtering	No	No	No	Yes	No	No	Yes	No	Yes	No	**Yes**
Re-breaking capability	No	No	Yes	Yes	Yes	No	No	Yes	No	Yes	**Yes**
Manual breaking operation	No	Yes	No	No	No	No	Yes	No	Yes	Yes	**Yes**
Stable breaking capability	No	No	No	No	No	No	No	No	No	Yes	**Yes**

[a] Inductors include discrete inductors and transformers.
[b] Values are obtained from the short-circuit fault results in the corresponding references.

TABLE IV
CHARACTERISTICS OF DIFFERENT COMPONENTS

Type	SCR	IGBT	GTO	IGCT	Diode
Code	*C783CC*	*FZ1500 R33HE3*	*5SGA 40L4501*	*5SHY 35L4520*	*VSSD11 00C32C*
Configuration	2 in parallel	2 in parallel	3 in parallel	2 in parallel	3 in parallel
ON-state voltage	1.50 V	3.45 V	2.75 V	1.9 V	1.30 V
Total costs	4.2 p.u.	17.1 p.u.	26.2 p.u.	21.8 p.u.	1.0 p.u.

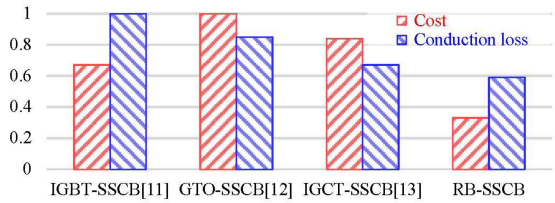

Fig. 15. Relative cost and conduction loss of four SSCBs.

structure. Furthermore, when compared with the existing SCR-SSCBs, the RB-SSCB can provide more reliable protection for dc microgrids mainly in three aspects.

1) *No current surges to the source and load sides*: During the fault breaking process, the RB-SSCB can totally eliminate current surges to the source and load sides, which can effectively protect the source and load, especially those composed of electronic devices, such as converters.
2) *Stable current breaking capability*: The current breaking capability of RB-SSCB is not affected by the parameters of the outer circuit. This means that despite changes in external circuit parameters (e.g., fault type and system structure), the breaker can still successfully interrupt the fault current. Consequently, the RB-SSCB can stably protect different dc microgrids from being damaged by various faults.
3) *Fully controllable breaking process*: The breaking process of the RB-SSCB is fully controllable because fault breaking, rebreaking and manual breaking operations can all be performed in the RB-SSCB. Hence, the RB-SSCB can provide comprehensive protection for dc microgrids.

B. Compared With SSCBs Based on Full-Controlled Devices

To make a more comprehensive comparison, this part further compares the RB-SSCB with the SSCBs based on IGBT [11], GTO [12], and IGCT [13] in the same power level. For intuitive comparison, the characteristics of the key components of the four SSCBs are listed in Table IV. Note that the components of the other three SSCBs are chosen according to the design guidelines provided in the corresponding references.

1) *Power loss evaluation:* For these four SSCBs, the conduction losses are mainly produced by one diode and one switch (SCR, IGBT, GTO, or IGCT). According to Table I, for the RB-SSCB, the conduction losses of 8.40 kW can be calculated. Furthermore, the SSCBs based on other commercial devices can also be calculated as 14.25 kW (IGBT-SSCB), 12.15 kW (GTO-SSCB), and 9.6 kW (IGCT-SSCB).
2) *Cost evaluation:* Since IGBT, GTO, and IGCT are full-controlled devices, the SSCBs based on these devices do not need additional commutating circuit to interrupt current . As a result, the total cost of these SSCBs is mainly composed of the cost of two switches (IGBT, GTO, or IGCT) and two diodes. According to Table I, total cost of the IGBT-SSCB, GTO-SSCB, and IGCT-SSCB can be calculated as 36.2 p.u., 54.4 p.u., and 45.6 p.u., respectively. For the RB-SSCB, the total cost mainly consists of the cost of three SCRs, three diodes, and one commutating capacitor (2.2 p.u.), which can be calculated as 17.8 p.u.

Furthermore, Fig. 15 gives the relative cost and conduction loss of these breakers, which indicates that the RB-SSCB has lower conduction loss and cost than the other three breakers, thus verifying the high efficiency and economical design of the RB-SSCB.

V. CONCLUSION

In this article, an RB-SSCB is proposed for dc microgrid protection. The RB-SSCB can provide low-pass voltage transfer

characteristic and interrupt bidirectional faults with no fault current surges to the source and load. Furthermore, its breaking capability is stable and controllable. As a result, when compared with the existing bidirectional breakers, the RB-SSCB can provide more reliable protection for dc microgrds. Also, the new solution retains the typical advantages in terms of high power efficiency, economical design, and simple structure. Design guidelines are presented based on detailed mathematical modeling and validated by the experimental results. The topology can be easily integrated into modern dc microgrids that require high supply reliability and high power efficiency.

REFERENCES

[1] C. Gamarra and J. M. Guerrero, "Computational optimization techniques applied to microgrids planning: A review," *Renewable Sustain. Energy Rev.*, vol. 48, no. 2/3, pp. 413–424, 2015.

[2] L. Yong *et al.*, "A virtual impedance comprehensive control strategy for the controllably inductive power filtering system," *IEEE Trans. Power Electron.*, vol. 32, no. 2, pp. 920–926, Feb. 2017.

[3] M. Rezkallah, S. Singh, B. Singh, A. Chandra, H. Ibrahim, and M. Ghandour, "Implementation of two-level coordinated control for seamless transfer in standalone microgrid," *IEEE Trans. Ind. Appl.*, vol. 57, no. 1, pp. 1057–1068, Jan./Feb. 2021.

[4] Y. Jeung, D. Lee, T. Dragičević, and F. Blaabjerg, "Design of passivity-based damping controller for suppressing power oscillations in DC microgrids," *IEEE Trans. Power Electron.*, vol. 36, no. 4, pp. 4016–4028, Apr. 2021.

[5] J. Peng, B. Fan, and W. Liu, "Voltage-based distributed optimal control for generation cost minimization and bounded bus voltage regulation in DC microgrids," *IEEE Trans. Smart Grid*, vol. 12, no. 1, pp. 106–116, Jan. 2021.

[6] S. Mirsaeidi *et al.*, "AC and DC microgrids: A review on protection issues and approaches," *IEEE J. Elect. Eng. Technol.*, vol. 12, no. 6, pp. 2089–2098, Feb. 2017.

[7] Z. J. Shen, Z. Miao, and A. M. Roshandeh, "Solid state circuit breakers for dc micrgrids: Current status and future trends," in *Proc. IEEE 1st Int. Conf. DC Microgrids*, 2015, pp. 228–233.

[8] X. Zhang *et al.*, "A state-of-the-art 500-kV hybrid circuit breaker for a dc grid: The world's largest capacity high-voltage DC circuit breaker," *IEEE Ind. Electron. Mag.*, vol. 14, no. 2, pp. 15–27, Feb. 2020.

[9] C. Peng, X. Song, A. Q. Huang, and I. Husain, "A medium-voltage hybrid DC circuit breaker—Part II: Ultrafast mechanical switch," *IEEE J. Emerg. Sel. Topics Power Electron.*, vol. 5, no. 1, pp. 289–296, Mar. 2017.

[10] J. Shu, S. Wang, J. Ma, T. Liu, and Z. He, "An active Z-source DC circuit breaker combined with SCR and IGBT," *IEEE Trans. Power Electron.*, vol. 35, no. 10, pp. 10003–10007, Oct. 2020.

[11] E. Haugan, H. Rygg, A. Skjellnes, and L. Barstad, "Discrimination in offshore and marine dc distribution systems," in *Proc. IEEE 17th Workshop Control Model. Power Electron.*, 2016, pp. 1–7.

[12] T. Genji, O. Nakamura, M. Isozaki, M. Yamada, T. Morita, and M. Kaneda, "400 V class high-speed current limiting circuit breaker for electric power system," *IEEE Trans. Power Del.*, vol. 9, no. 3, pp. 1428–1435, Jul. 1994.

[13] Q. Lu *et al.*, "Design and analysis of a 375V/5kA solid state DC circuit breaker based on IGCT," in *Proc. IEEE Int. Power Electron. Appl. Conf. Expo.*, 2018, pp. 1–5.

[14] D. P. Urciuoli, V. Veliadis, H. C. Ha, and V. Lubomirsky, "Demonstration of a 600-V, 60-A, bidirectional silicon carbide solid-state circuit breaker," in *Proc. 26th Annu. IEEE Appl. Power Electron. Conf. Expo.*, 2011, pp. 354–358.

[15] Z. J. Shen *et al.*, "First experimental demonstration of solid state circuit breaker (SSCB) using 650 V GaN-based monolithic bidirectional switch," in *Proc. 28th Int. Symp. Power Semicond. Devices ICs*, 2016, pp. 79–82.

[16] X. Xu, W. Chen, C. Liu, R. Sun, Z. Li, and B. Zhang, "An efficient and reliable solid-state circuit breaker based on mixture device," *IEEE Trans. Power Electron.*, vol. 36, no. 9, pp. 9767–9771, Sep. 2021.

[17] J. Shu, J. Ma, S. Wang, Y. Dong, T. Liu, and Z. He, "A new active thyristor-based DCCB with reliable opening process," *IEEE Trans. Power Electron.*, vol. 36, no. 4, pp. 3617–3621, Apr. 2021.

[18] P. M. McEwan and S. B. Tennakoon, "A two-stage dc thyristor circuit breaker," *IEEE Trans. Power Electron.*, vol. 12, no. 4, pp. 597–607, Jul. 1997.

[19] W. Chen *et al.*, "Evaluation of CS-MCT in dc solid state circuit breaker (SSCB) applications," *IEEE Trans. Ind. Appl.*, vol. 54, no. 5, pp. 5465–5473, Oct. 2018.

[20] K. A. Corzine, "A new-coupled-inductor circuit breaker for dc applications," *IEEE Trans. Power Electron.*, vol. 32, no. 2, pp. 1411–1418, Feb. 2017.

[21] A. H. Chang, B. R. Sennett, A. Avestruz, S. B. Leeb, and J. L. Kirtley, "Analysis and design of dc system protection using Z-source circuit breaker," *IEEE Trans. Power Electron.*, vol. 31, no. 2, pp. 1036–1049, Feb. 2016.

[22] K. A. Corzine and R. W. Ashton, "A new Z-source dc circuit breaker," *IEEE Trans. Power Electron.*, vol. 27, no. 6, pp. 2796–2804, Jun. 2012.

[23] D. J. Ryan, H. D. Torresan, and B. Bahrani, "A bidirectional series Z-Source circuit breaker," *IEEE Trans. Power Electron.*, vol. 33, no. 9, pp. 7609–7621, Sep. 2018.

[24] D. Keshavarzi, T. Ghanbari, and E. Farjah, "A Z-source based bidirectional dc circuit breaker with fault current limitation and interruption capabilities," *IEEE Trans. Power Electron.*, vol. 32, no. 9, pp. 6813–6822, Sep. 2017.

[25] S. Savaliya and B. G. Fernandes, "Comparative analysis and coordination study of bi-directional Z-source breaker with reclosing capabilities," in *Proc. 19th Eur. Conf. Power Electron. Appl.*, 2017, pp. P.1–P.10.

[26] A. Maqsood and K. Corzine, "The Z-source breaker for ship power system protection," in *Proc. IEEE Electr. Ship Technol. Symp.*, 2015, pp. 293–298.

[27] A. Maqsood and K. Corzine, "The Z-source breaker for fault protection in ship power systems," in *Proc. Int. Symp. Power Electron., Elect. Drives, Automat. Motion*, 2014, pp. 307–312.

[28] Y. Wang, W. Li, X. Wu, and X. Wu, "A novel bidirectional solid-state circuit breaker for dc microgrid," *IEEE Trans. Ind. Electron.*, vol. 66, no. 7, pp. 5707–5714, Jul. 2019.

[29] Z. Zhou, J. Jiang, S. Ye, C. Liu, and D. Zhang, "A Γ-source circuit breaker for DC microgrid protection," *IEEE Trans. Ind. Electron.*, vol. 68, no. 3, pp. 2310–2320, Mar. 2021.

[30] S. G. Savaliya and B. G. Fernandes, "Modified bi-directional Z-source breaker with reclosing and rebreaking capabilities," in *Proc. IEEE Appl. Power Electron. Conf. Expo.*, 2018, pp. 3497–3504.

[31] S. G. Savaliya and B. G. Fernandes, "Performance evaluation of a modified bidirectional Z-source breaker," *IEEE Trans. Ind. Electron.*, vol. 68, no. 8, pp. 7137–7145, Aug. 2021.

[32] Z. Zhou, J. Jiang, S. Ye, D. Yang, and J. Jiang, "Novel bidirectional O-Z-source circuit breaker for DC microgrid protection," *IEEE Trans. Power Electron.*, vol. 36, no. 2, pp. 1602–1613, Feb. 2021.

[33] Z. Zhou, M. Chen, J. Jiang, D. Zhang, S. Ye, and C. Liu, "Analysis and design of a novel thyristor-based circuit breaker for dc microgrids," *IEEE Trans. Power Electron.*, vol. 35, no. 3, pp. 2959–2968, Mar. 2020.

[34] X. Xu, W. Chen, H. Tao, Q. Zhou, Z. Li, and B. Zhang, "Design and experimental verification of an efficient SSCB based on CS-MCT," *IEEE Trans. Power Electron.*, vol. 35, no. 11, pp. 11682–11693, Nov. 2020.

[35] F. Zhang, Y. Ren, Z. Shi, X. Yang, and W. Chen., "Novel hybrid DC circuit breaker based on series connection of thyristors and IGBT half-bridge submodules," *IEEE Trans. Power Electron.*, vol. 36, no. 2, pp. 1506–1518, Feb. 2021.

[36] G. Ebner, W. Hartmann, M. Hergt, and S. Wietzel, "Fault arc extinction and system re-start on HVDC transmission lines using LCC or VSC full-bridge converters with integrated arc recovery simulation models," in *Proc. 13th IET Int. Conf. AC DC Power Transmiss.*, 2017, pp. 1–5.

[37] G. Parlangeli, "An adaptive D-FACTS for power quality enhancement in an isolated microgrid," *IEEE Access*, vol. 8, pp. 98775–98786, 2020.

[38] L. Qi *et al.*, "Solid-state circuit breaker protection for DC shipboard power systems: Breaker design, protection scheme, validation testing," *IEEE Trans. Ind. Appl.*, vol. 56, no. 2, pp. 952–960, Mar./Apr. 2020.

[39] S. Ahmadi, I. Sadeghkhani, G. Shahgholian, B. Fani, and J. Guerrero, "Protection of LVDC microgrids in grid-connected and islanded modes using bifurcation theory," *IEEE J. Emerg. Sel. Topics Power Electron.*, vol. 9, no. 3, pp. 2597–2604, Jun. 2021.

[40] F. Alhuwaishel, A. Allehyani, S. Al-Obaidi, and P. Enjeti, "A medium-voltage DC-collection grid for large-scale PV power plants with interleaved modular multilevel converter," *IEEE J. Emerg. Sel. Topics Power Electron.*, vol. 8, no. 4, pp. 3434–3443, Dec. 2020.

[41] T. Dragičević, X. Lu, J. C. Vasquez, and J. M. Guerrero, "DC microgrids—Part II: A review of power architectures applications and standardization issues," *IEEE Trans. Power Electron.*, vol. 31, no. 5, pp. 3528–3549, May 2016.